J. Comput. Appl. Res. Mech. Eng. Vol. 13. No. 1, pp. 13-25, 2023 *DOI: 10.22061/JCARME.2023.8916.2202*

Journal of Computational and Applied Research in Mechanical Engineering

jcarme.sru.ac.ir

SRTTU

JCARME

ISSN: 2228-7922

Research paper

3D numerical analysis of arterial thromboembolism through carotid bifurcation

Pouria Talebibarmi and Bahman Vahidi*

Faculty of New Sciences and Technologies, University of Tehran, Tehran, Iran

Article info:

Article history:

Received: 27/03/2022

Accepted: 02/05/2023

Revised: 06/05/2023

Online: 09/05/2023

Keywords:

Arterial embolism,
Ischemic stroke,
Fluid-solid interaction,
Visco-hyperelastic model,
Wall shear stress.

***Corresponding author:**
bahman.vahidi@ut.ac.ir

Abstract

Arterial embolism is one of the major causes of brain infarction. Investigating the hemodynamic factors of this phenomenon can help us to get a better understanding of this complication. The carotid artery is one of the primary tracts that emboli can go toward the brain through it. In this study, we used a 3D model of the carotid bifurcation, and two geometries, elliptical and spherical, were considered for the clots. Hyperelastic and visco-hyperelastic models were used for the mechanical properties of clots. The governing equations of the fluid are Navier-Stokes and continuity equations and have been solved in an Arbitrary Lagrangian-Eulerian (ALE) formulation through the fluid-structure interaction method. The hemodynamic parameters of fluid and shear stress on the wall of the carotid artery were calculated. Besides, by using ADINA software, the effective stress (Von Mises stress) of the clots and the shear stress created on them were evaluated as well. Results revealed that the elliptical clot has more effects on the hemodynamic parameters of the fluid, and the mechanical property of clots has significant effects on the amount of stress created on the clots. Also, clot fracture will not occur due to the point that the maximum effective stress in this study was 1819 Pa but the creation of crack in clots is more probable, and this probability is more for the elliptical clot.

1. Introduction

A stroke is a brain lesion that results in a lack of blood supply to the brain cells (lack of glucose and oxygen as nutrients) and the death of tissue in that area of the brain. In general, strokes are divided into 3 types: transient stroke, ischemic stroke, and hemorrhagic stroke [1]. In particular, in ischemic stroke, a blood clot or mass clogs the arteries, which are usually embolic and thrombotic Ischemic. In a thrombotic stroke, a clot is formed inside one of the brain's arteries, and when a blood clot is formed elsewhere in the body and moves toward the brain is called an embolic stroke [2]. Arterial bifurcations and narrowed areas caused by atherosclerosis are common places for appearing embolisms. The reason for narrowing arteries in atherosclerosis is the developing cholesterol-filled plaques in the walls of arteries [3, 4]. The emboli can be air bubbles, fat pieces, or platelets [5]. Since embolic stroke is one of the most important causes of mortality in the world, knowledge of the mechanism of embolism function and the

effective parameters in causing stroke due to arterial embolism can be very effective in improving the treatment methods of this complication. To achieve these goals, researchers use animal models, laboratory models, and computational models that due to the limitations of laboratory methods such as the inability to study several parameters simultaneously and the cost of testing, computational models are more important. In previous studies, Bushi et al. [6] evaluated the embolic trajectory in the carotid artery and the effects of particles size and fluid density on particles distribution. Vahidi *et al*. [7] considered a numerical analysis of a fully blocked human common carotid artery due to the thromboembolism phenomenon of the arterial embolism by using a contact finite element model. In another study by Vahidi and Fatouraee [8], a symmetric axial computational model was developed for the embolism movement with different diameters in clogged arteries. They analyzed the effect of the size and density of an embolus on its trajectory and movement. In the study by Fabbri *et al*. [9], using numerical modeling, they investigated the effect of particle size and mass on path selection in the carotid and basilar arteries. Mukherjee *et al*. [10] stated how embolus size and other factors affect embolus distribution in the brain.

In the previous investigations, the effects of the clot's geometries were not considered and in all of them, the clots were assumed spherical. Therefore, we decided to evaluate the effects of this parameter on the hemodynamic parameters of fluid flow and stresses created on the emboli. To do this, two geometries, spherical and elliptical, were assumed for the clot and compared with each other. also, hyperelastic and visco-hyperelastic models were considered for the mechanical properties of the clots to evaluate the effects of viscosity on clot structure. According to this point that heart pulse pressure was used as input, the time of clot presence in carotid bifurcation can be a valuable parameter for analysis. To evaluate this parameter, the clots were released at the beginning of the systole and the peak of the systole.

2. Materials and methods

Here a computational simulation was used to investigate the effects of emboli geometries and their mechanical properties on the mechanism of thromboembolism in the carotid bifurcation. To analyze this issue, two geometries, spherical and elliptical, were used for emboli geometries, and hyperelastic and visco-hyperelastic models were used for their mechanical properties. A 3D rigid model [11] of the carotid bifurcation was used and its geometrical features were compatible with the models that were used in previous works [12-14]. The dimensions of the emboli and the carotid bifurcation are shown in Fig. 1. [12]. To achieve fully developed fluid flow, entry length was considered long enough (not shown in Fig. 1). To evaluate the effects of embolus releasing time, two release times, the beginning and peak of the systole, were simulated.

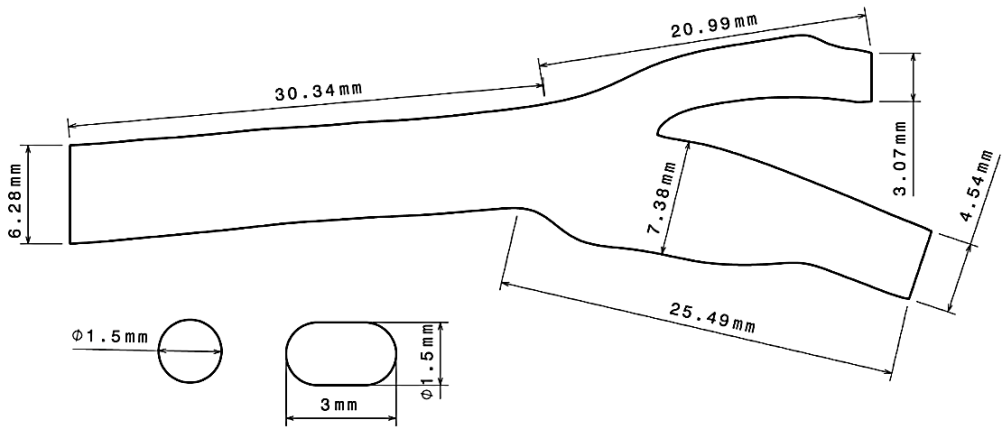

Fig. 1. The carotid bifurcation and the clots dimensions.

2.1. Blood and embolus material properties

The blood was considered Newtonian [15], viscous, and incompressible with a viscosity of 3.48 cP and a density of 1054 $kg\,m^3$[16]. It is an approved assumption that blood behaves like a Newtonian fluid in situations in which the shear rate is above 100 s^{-1} [1, 17]. The density of the emboli was assumed to equal the blood density according to previous works [1, 9]. The Mooney- Rivlin model based on the stress-strain curve reported by Xie *et al.* [18] was considered for the mechanical properties of emboli. To add the viscoelastic feature to our models, we used the generalized Maxwell model. This model is suitable for representing viscoelastic materials like living tissues [19]. The stress formula in terms of viscoelastic coefficients is brought in Eq. (1) [19].

$$\sigma = \int_0^t E^{\infty}\left[1 + \sum_a \beta^a \; exp\left(-\frac{t-t'}{\tau^a}\right)\right] e \cdot dt' \tag{1}$$

$$\tau^{\alpha} = \frac{\eta^{\alpha}}{E^{\alpha}} \tag{2}$$

$$\beta^{\alpha} = \frac{E^{\alpha}}{E^{\infty}} \tag{3}$$

where τ and β are the viscoelastic material constants and t, η, E, and σ are time, viscosity, elasticity, and stress in the generalized Maxwell model, respectively (Table 1) [19].

2.2. Numerical domains and governing equations

The tetrahedral mesh was used for both the carotid bifurcation and the emboli that their discretized geometries are shown in Fig. 2(a). For the grid independence study, three models with different element numbers, 55066, 85599, and 89078 were considered for the fluid region, and the wall shear stress near the bifurcation in presence of the spherical clot was evaluated [20]. The difference between the first and second models was 10% and between the second and third models was 2%. Therefore, the second model was used in our simulation. Here, the number of elements for spherical and elliptical clots, and their corresponding fluid regions were 92, 216, 85599, and 85475, respectively. In this study, ALE formulation was used for fluid model. The conservation of mass and momentum in ALE form are summarized in below Eqs. (4-6) [21]:

$$\left.\frac{\partial \rho}{\partial t}\right|_{\chi} + c \cdot \nabla \rho = -\rho \nabla \cdot v \tag{4}$$

$$\rho\left(\left.\frac{\partial v}{\partial t}\right|_{\chi} + (c \cdot \nabla)v\right) = \nabla \cdot \sigma + \rho b \tag{5}$$

$$c = v - \hat{v} \tag{6}$$

where t is the time, ρ is the density, $|_{\chi}$ means that "holding the referential coordinate χ fixed", v represents material velocity, b is specific body force, σ is Cauchy stress tensor and $\hat{v}$ is mesh velocity.

General Lagrangian formulation was used for structural model. Motion equation and the fluid force which exerted on the structure are brought in below, respectively Eqs. (7, 8) [22, 23]:

$$\frac{\partial \mathrm{L}}{\partial q_i} - \frac{d}{dt}\frac{\partial \mathrm{L}}{\partial \dot{q}_i} = 0 \tag{7}$$

$$F(t) = \int h^d \tau_f \cdot dS \tag{8}$$

where h^d is virtual quantity of the solid displacement and τ_f is the fluid stress.

Table 1. Mechanical properties of the blood clot [19].

$E^{\infty}\,(Pa)$	$E^1\,(Pa)$	$E^2\,(Pa)$	$\eta^1\,(Pa,s)$	$\eta^2\,(Pa,s)$	$\tau^1\,(s)$	$\tau^2\,(s)$	β^1	β^2	$\rho\,(kg/m^3)$
518.42	1.3e15	748.66	0.13	2.95	0.1e-15	0.00394	0.25e13	1.444	1054

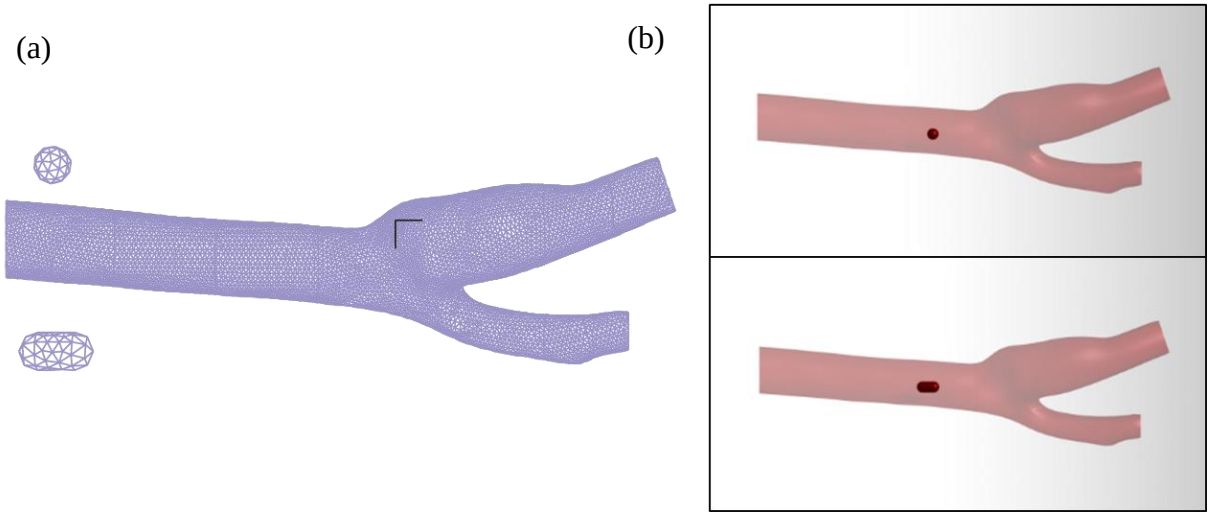

Fig. 2. (a) Discritized geometries of the clots and carotid bifurcation, and (b) initial position of the both clots.

2.3. Boundary conditions

The heart pulse pressure pattern [24] was used as the inlet boundary condition which the maximum amount of it was 480 Pa, and zero normal traction was considered as the outlet boundary condition [1]. To validate the inlet and outlet boundary condition, a model without the presence of emboli was simulated and its hemodynamic parameters like fluid velocity and wall shear stress were compared with previous work [25]. No-slip boundary condition was applied at the walls [26], and the FSI condition was defined between the embolus and blood on their interface. The contact condition was modeled between the wall of the artery (target surface) and the emboli (contactor surface). The offset between the contact surface was 0.2 mm, and 0.0001 was utilized for the compliance factor. First, the clot was fixed at the center of the artery before bifurcation Fig. 2(b) by defining spring elements that were applied to clot surrounding nodes. After passing some time step, the spring elements were removed, and let the clot moved inside the artery.

2.4. Solution methods

In this study, the fluid-structure interaction (FSI) was employed, and the finite element package ADINA (Adina R&D Inc., Watertown MA, USA version 9.6) was used to solve the coupled fluid and structure models. When any part of the computational domain is deformable, the Eulerian description of fluid is not applicable anymore so the Arbitrary-Lagrangian-Eulerian formulation (ALE) was employed in this simulation that comprises both the Eulerian and the Lagrangian description of fluid. During moving the clot through the fluid domain, the fluid mesh will be distorted and make the simulation to stop, so the steered adaptive mesh modification process was used that refined the fluid mesh in the simulation. The solver which was exerted in this study was the sparse solver based on Gauss elimination. As the direct computational two-way coupling method is faster than the iterative method, it was used in this study. In this method, the fluid and structure equations are combined and treated in one system. The Newton-Raphson iterative method was used in our simulations for solving discretized fluid and structure equations. Here, 500 iterations per step were applied for both fluid and structure models. A magnitude of 0.8 was used for force and displacement relaxation factors, and 0.01 was used for relative force and displacement tolerances.

3. Results and discussion

3.1. Flow hemodynamics

The fluid velocity in the plane crossing both spherical and elliptical embolus is shown in Fig. 3. It is obvious that the fluid velocity is higher

in the middle of the lumen before arriving at the bifurcation. Near the bifurcation, the velocity of fluid decreases and then increases after passing the bifurcation. Based on the resent results, the velocity magnitude in the carotid artery and its branches in the presence of an elliptical clot is lower than in the presence of a spherical clot. Both clots go toward the larger branch, as shown in previous work [12]. The maximum fluid velocity in our simulations was 0.5132 m/s which was in the physiological range [25]. The pressure gradient is shown in Fig. 4, as both clots got close to the bifurcation, the pressure gradient increased at their front and decreased the clot velocity, and then when they passed the bifurcation, their velocity increased.

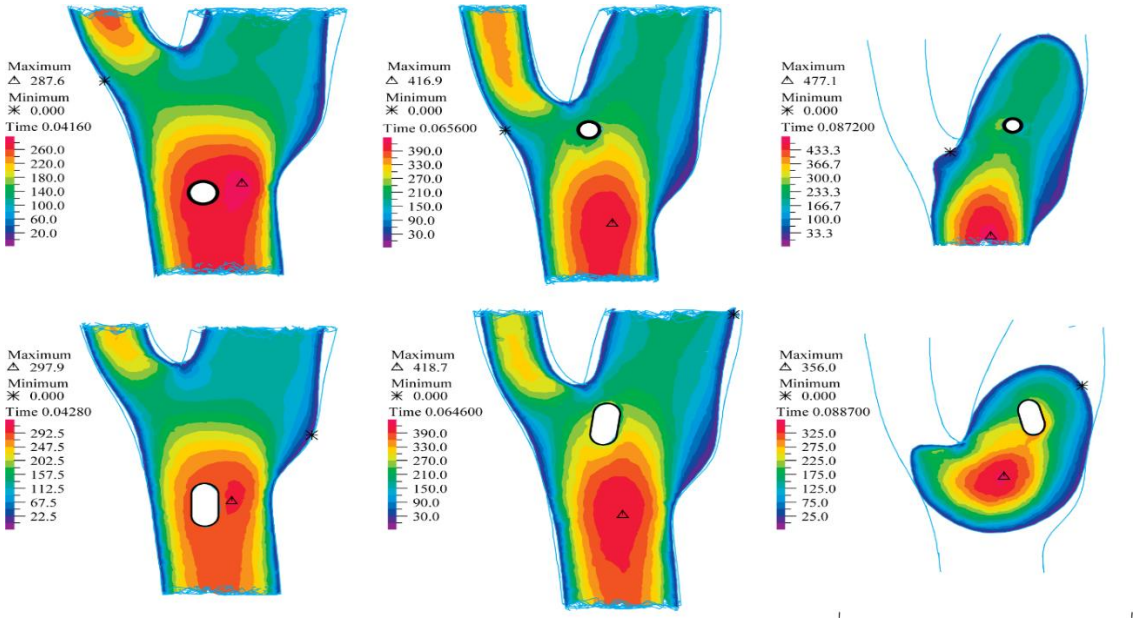

Fig. 3. Velocity magnitude of fluid (mm/s).

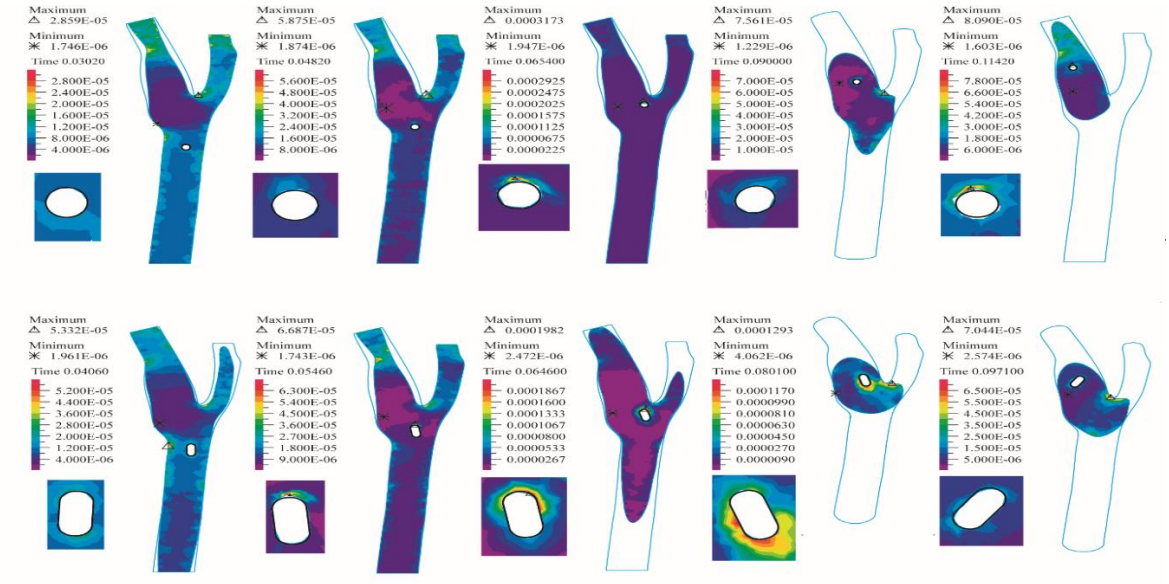

Fig. 4. Pressure gradient in fluid field (N/mm^3).

The pressure gradient around the elliptical clot made it rotate in the fluid flow and had more effects on the fluid contour in comparison with the spherical clot.

3.2. Arterial wall shear stress

The arterial wall shear stress is shown in Fig. 5. As it is obvious from the picture, passing the fluid through the smaller branch applied higher shear stress on the arterial wall. The maximum magnitude of wall shear stress in this study was approximately 5 Pa, which was in the physiological range that was reported in previous works [12, 25]. To show the influences of emboli presence, two models, with and without presence of emboli, were simulated and the obtained results were compared. According to what we said about the effects of emboli on the fluid velocity magnitude, the presence of emboli in the artery caused decreasing in arterial wall shear stress. As expected, the presence of the elliptical clot had more influence on the wall shear stress, and in this situation, the arterial wall tolerated lower stress. Continuance of this situation can lead to damage to endothelial surface cells [27]. In fact, the abnormal distribution of shear stress plays an important role in diseases such as atherosclerosis and aneurysm [28].

3.3. Stress on the embolus

Plots of average shear stress on the emboli surface are shown in Fig. 6. According to the plots, the spherical clot collided with the arterial wall once, but the elliptical clot collided with the arterial wall three times.
The shear stress on the clots and effective stress at the contact points with the arterial wall is shown in Figs. 7-8. In Figs. 9-10, the shear stress on the clot and its trajectory are shown for both clots. As both clots got close to the bifurcation, the magnitude of shear stress and effective stress increased in both clots. In the case of releasing the clots at the peak of the systole, the magnitude of shear stress and effective stress of the clots at their first contact with the wall was higher than when the clots were released at the beginning of the systole.

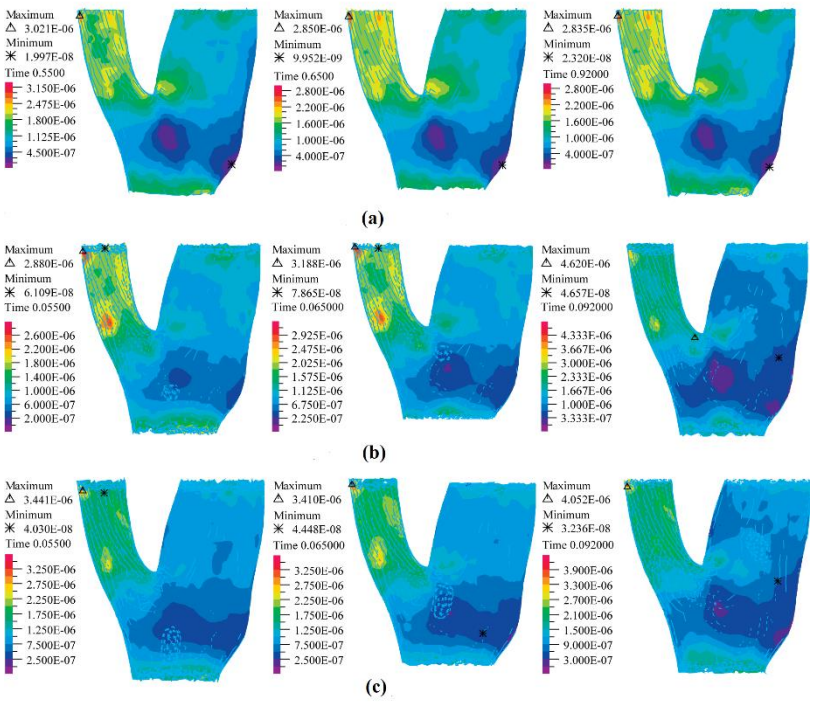

Fig. 5. Comparison of wall shear stress in the carotid bifurcation in presence of (a) the spherical (b) the elliptical clots and (c) without the presence of any emboli (N/mm^2).

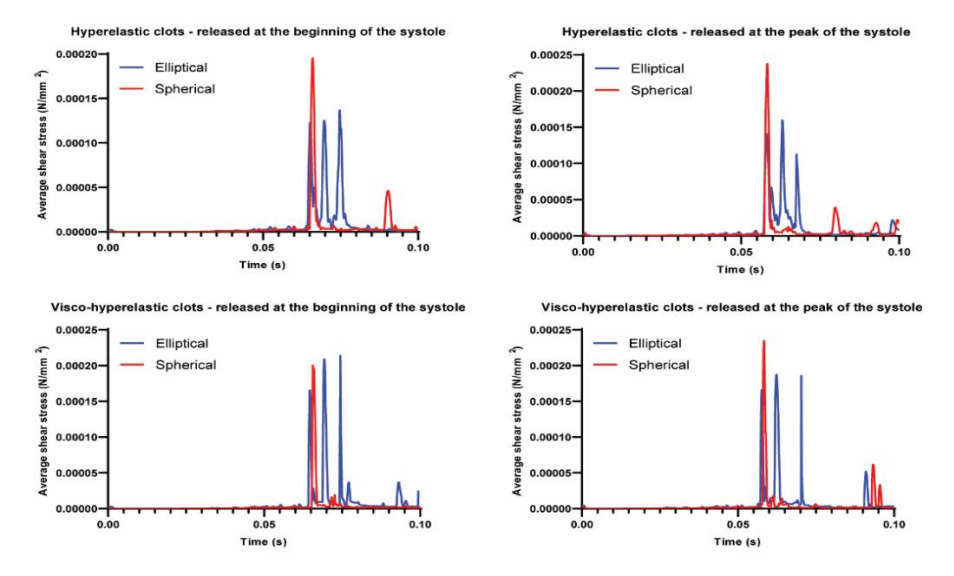

Fig. 6. Average shear stress on the elliptical and the spherical clots surface.

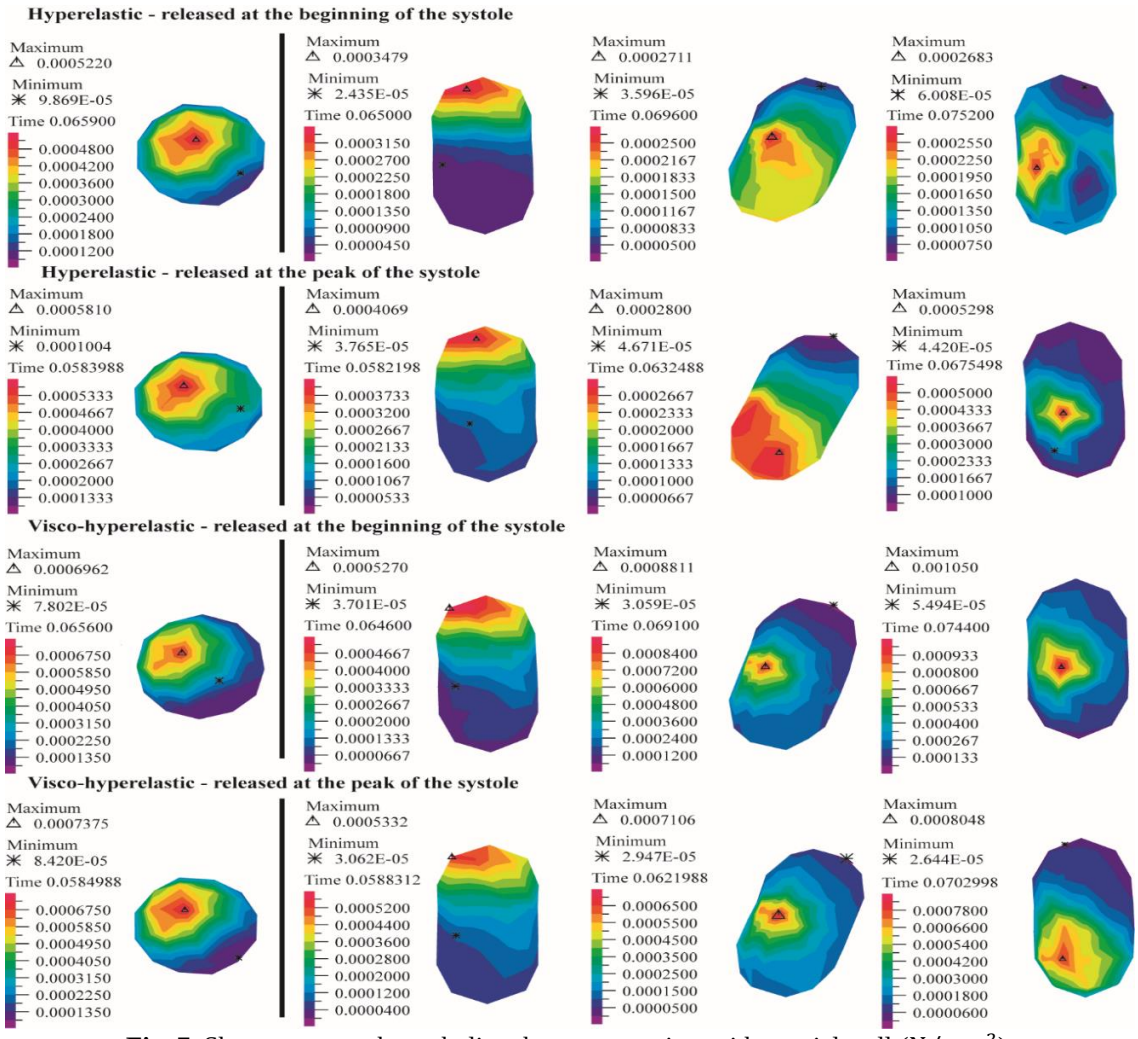

Fig. 7. Shear stress on the emboli at the contact points with arterial wall (N/mm^2).

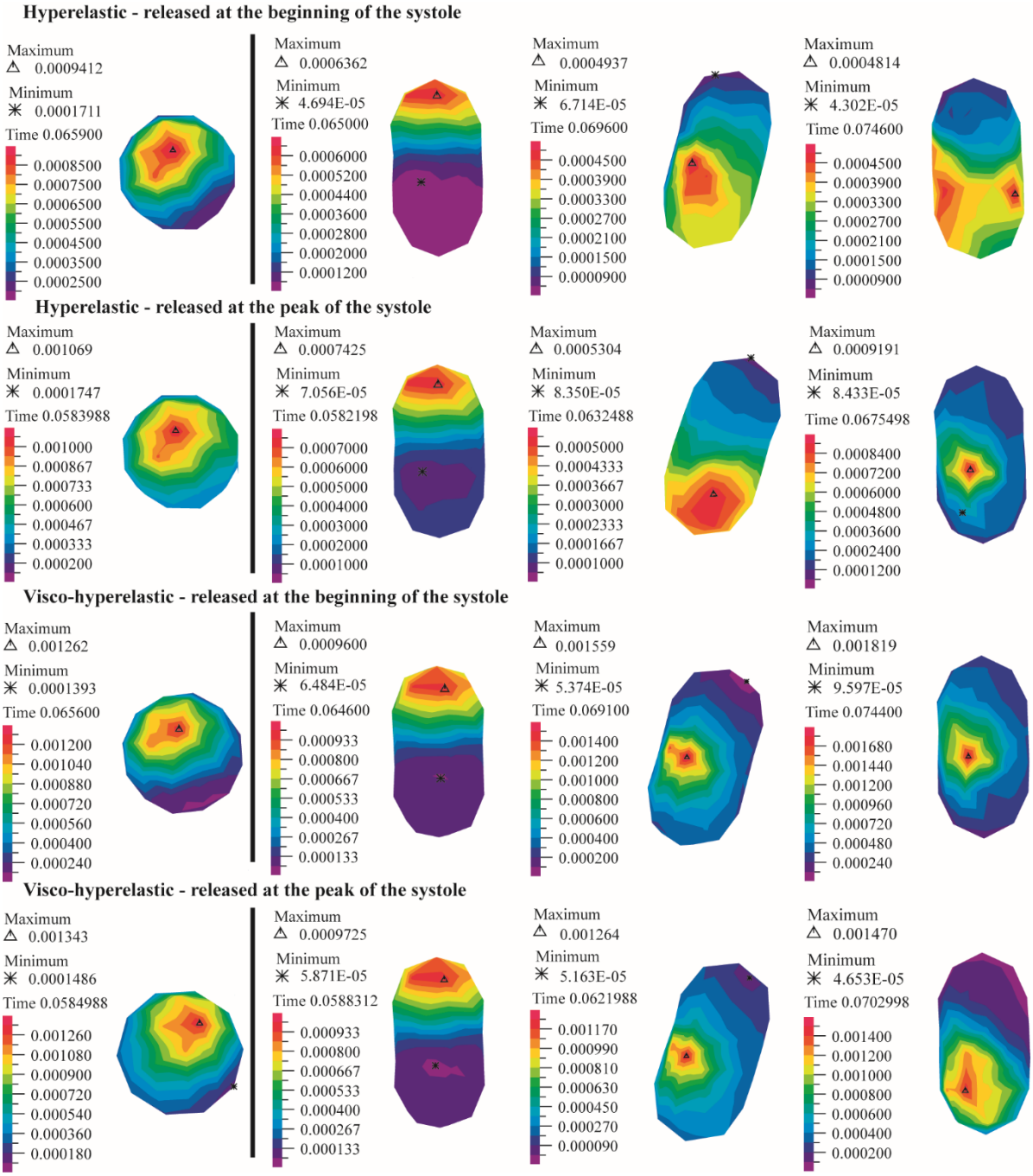

Fig. 8. Effective stress of the emboli at the contact point with arterial wall (N/mm^2).

Visco-hyperelastic clots experienced higher stress than hyperelastic clots at the collision moment with the bifurcation. Visco-hyperelastic materials, due to their viscosity, are strain-rate dependent and respond differently depending on how fast the force is applied to them. They behave like stiff solids in situations with fast strain rates [29]. Therefore, the reason for this difference between stress magnitudes in which clots were experienced at their contact point with bifurcation could be this feature of visco-hyperelastic materials. According to a previous study by Tutwiler *et al*. [30], clots with cracks are more vulnerable to rupture, and they reported that shear stress of more than 1 kPa can create cracks in clots.

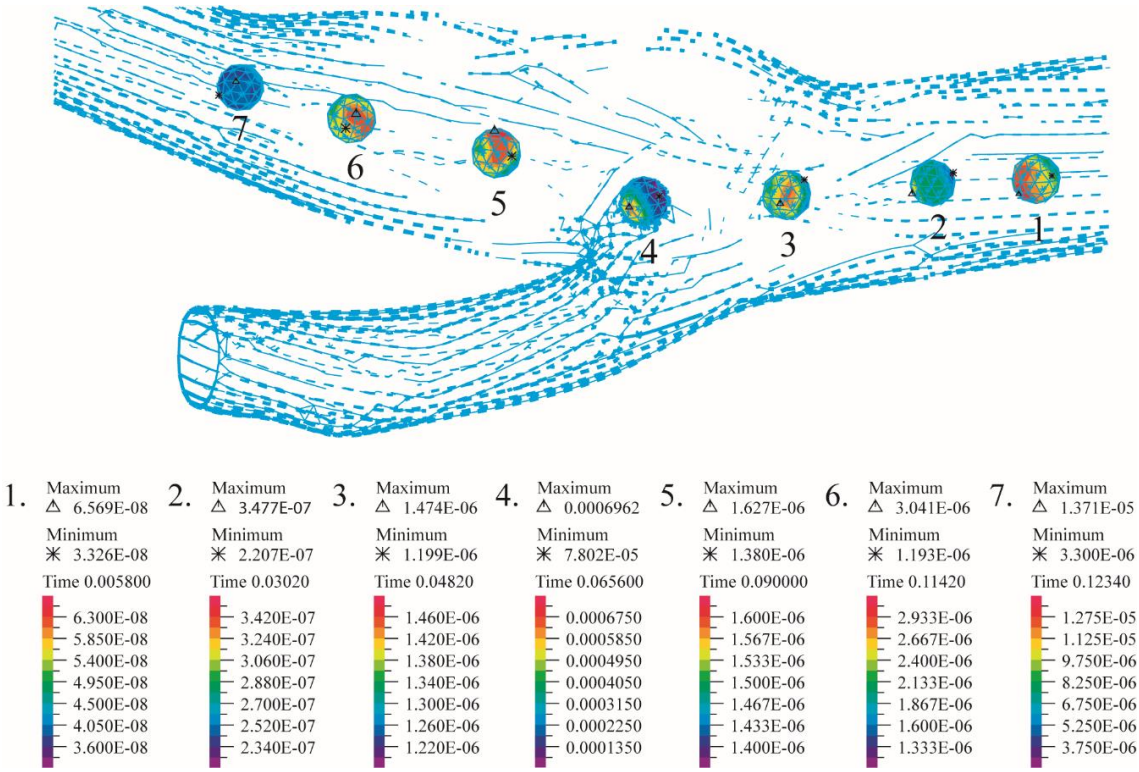

Fig. 9. The spherical clot trajectory and maximum shear stress on it (N/mm^2).

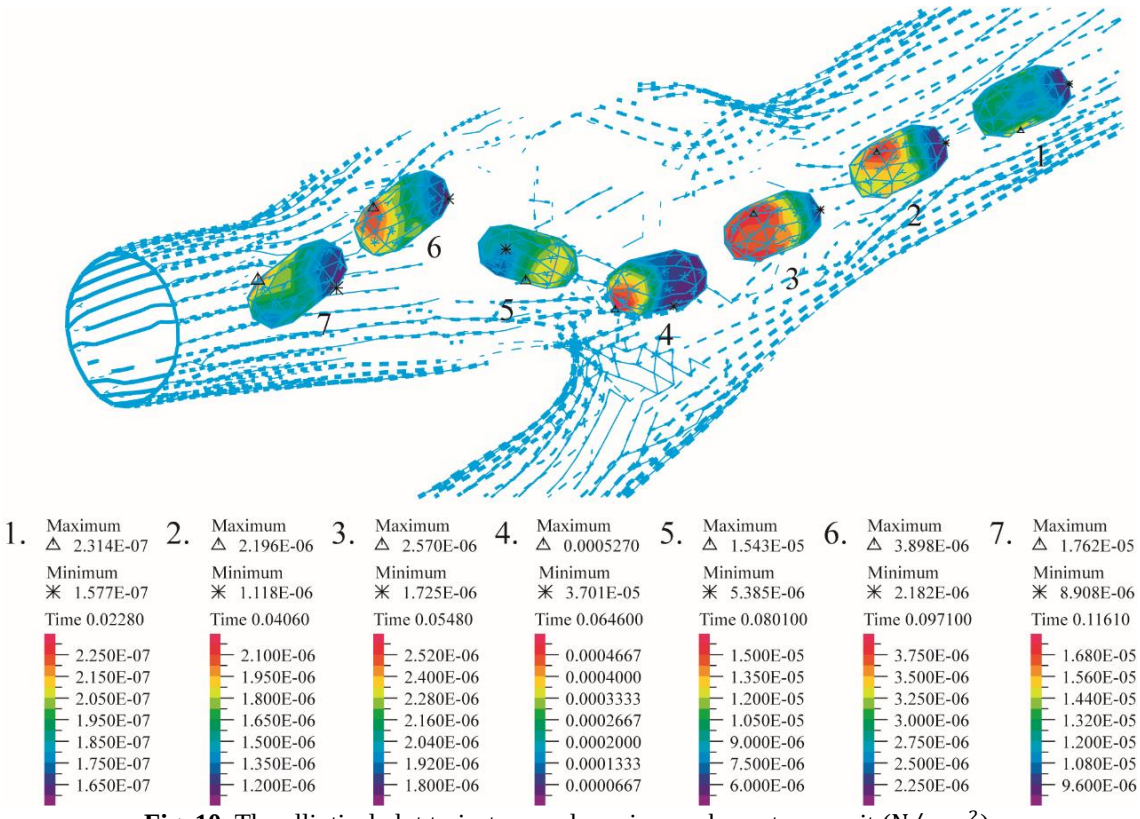

Fig. 10. The elliptical clot trajectory and maximum shear stress on it (N/mm^2).

Table 2. Maximum amount of the shear stress and effective stress.

No	Model	Mechanical property	Release time (s)	Max shear stress (Pa)	Max effective stress (Pa)
1	Spherical	Hyperelastic	Beginning of the systole	522	941.2
2	Spherical	Hyperelastic	Peak of the systole	581	1069
3	Elliptical	Hyperelastic	Beginning of the systole	347.9	636.2
4	Elliptical	Hyperelastic	Peak of the systole	529.8	919.1
5	Spherical	Visco-hyperelastic	Beginning of the systole	696.2	1262
6	Spherical	Visco-hyperelastic	Peak of the systole	737.5	1343
7	Elliptical	Visco-hyperelastic	Beginning of the systole	1050	1819
8	Elliptical	Visco-hyperelastic	Peak of the systole	804.8	1470

In another study by Liu *et al.* [31], it was reported that the yield stress of clots based on their composition ranged from 63 – 2396 kPa. The maximum shear stress and effective stress in our study are brought in Table 2. According to the previous work [12], the magnitude of shear stress on the clots in this study was acceptable. As regards the maximum effective stress in our results was 1819 Pa, none of the clots received their ultimate stress, but the amount of maximum shear stress on clots in our results was near 1 kPa, so the possibility of crack creation in clots would be more probable. In this study, the elliptical clots were exposed to high shear stress for longer compared to spherical clots. So, the elliptical clots are more likely to crack and rupture, and the risk of them will be decreased because the probability of large vessel occlusion will be decreased [32].

4. Limitations and future works

To decrease the cost and time of the present simulation, two geometries were considered for the emboli. In addition, the release position of the clots was at the center of the artery. Other positions, like near the artery wall, could be considered in future studies. To close the simulation to real and improve its accuracy, using real geometry of the carotid artery based on medical images, and considering its mechanical property could be helpful. Furthermore, we assumed the blood as a Newtonian fluid that its non-Newtonian feature is worthy to be evaluated in future studies as discussed in the former reports [25, 33]. To get a better understanding of the effects of clots' geometries and their mechanical properties, using geometries that are more similar to real clots and considering different mechanical properties based on their sources seems to be valuable. Studying the effects of the presence of several emboli in the blood flow and other types of emboli, such as gas emboli could be investigated in future works.

5. Conclusions

As stroke is one of the most important reasons for mortality, investigating this phenomenon are of great importance. In this study, the fluid-structure interaction method was used to evaluate the effects of clot geometry, time release of the clots, and their mechanical properties on the mechanism of the embolism. These kinds of studies could be useful to decrease the cost of investigations and could help to evaluate the effects of several parameters at the same time. In previous studies, spherical geometry was used for modeling the clots and the effect of viscosity on clot mechanical properties, and the influence of clots present in the carotid artery was not evaluated. Therefore, the present simulations extend previous observations. It was shown that the geometry of clots has a significant influence on the hemodynamic flow and the stresses created on the embolus. Furthermore, it was shown that the mechanical properties of the emboli and their releasing time have impressive effects on the stresses on clots. For example, the elliptical clot modeled as a visco-hyperelastic material experienced the highest amount of effective stress (1819 Pa) in comparison with other models in our study and was more vulnerable to rupture. This study can help to get a better understanding of embolism that could be useful to cure this phenomenon.

6. References

[1] F. Khodaee, B. Vahidi and N. Fatouraee, "Analysis of mechanical parameters on the thromboembolism using a patient-specific computational model," *Biomech. Model. Mechanobiol*, Vol. 15, No. 5, pp. 1295-1305, (2016).

[2] G. Ntaios and R. G. Hart, "Embolic stroke," *Circulation*, Vol. 136, No. 25, pp. 2403-2405, (2017).

[3] M. Coggia, O. Goëau-Brissonnière, J.-L. Duval, J.-P. Leschi, M. Letort, and M.-D. Nagel, "Embolic risk of the different stages of carotid bifurcation balloon angioplasty: an experimental study," *J. Vasc. Surg.*, Vol. 31, No. 3, pp. 550-557, (2000).

[4] J. Xiang, T. Zhang, Q.-w. Yang, J. Liu, Y. Chen, M. Cui, Z.-G. Yin, L. Li, Y.-J. Wang and J. Li, "Carotid artery atherosclerosis is correlated with cognitive impairment in an elderly urban Chinese non-stroke population," *J. Clin. Neurosci.*, Vol. 20, No. 11, pp. 1571-1575, (2013).

[5] M. Appelblad and G. Engström, "Fat contamination of pericardial suction blood and its influence on in vitro capillary-pore flow properties in patients undergoing routine coronary artery bypass grafting," *J. Thorac. Cardiovasc. Surg.*, Vol. 124, No. 2, pp. 377-386, (2002).

[6] D. Bushi, Y. Grad, S. Einav, O. Yodfat, B. Nishri and D. Tanne, "Hemodynamic evaluation of embolic trajectory in an arterial bifurcation: an in-vitro experimental model," *Stroke*, Vol. 36, No. 12, pp. 2696-2700, (2005).

[7] B. Vahidi and N. Fatouraee, "Numerical analysis of fully blocked human common carotid artery resulted from arterial thromboembolism using a contact finite element model," *Iran. Biomed. J.*, Vol. 2, No. 4, pp. 285-296, (2009).

[8] B. Vahidi and N. Fatouraee, "Large deforming buoyant embolus passing through a stenotic common carotid artery: A computational simulation," *J. Biomech.*, Vol. 45, No. 7, pp. 1312-1322, (2012).

[9] D. Fabbri, Q. Long, S. Das and M. Pinelli, "Computational modelling of emboli travel trajectories in cerebral arteries: influence of microembolic particle size and density," *Biomech. Model. Mechanobiol.*, Vol. 13, No. 2, pp. 289-302, (2014).

[10] D. Mukherjee, J. Padilla and S. C. Shadden, "Numerical investigation of fluid–particle interactions for embolic stroke," *Theor. Comput. Fluid. Dyn.*, Vol. 30, No. 1, pp. 23-39, (2016).

[11] E. Miranda, L. C. Sousa, C. C. António, C. F. Castro and S. I. S. Pinto, "Role of the left coronary artery geometry configuration in atherosusceptibility: CFD simulations considering sPTT model for blood," *Comput Methods Biomech Biomed Engin*, Vol. 24, No. 13, pp. 1488-1503, (2021).

[12] E. Abolfazli, N. Fatouraee and B. Vahidi, "Dynamics of motion of a clot through an arterial bifurcation: a finite element analysis," *Fluid Dyn. Res.*, Vol. 46, No. 5, p. 055505, (2014).

[13] S. Tada, "Computational study of the influence of bifurcation angle on haemodynamics and oxygen transport in the carotid bifurcation," *Biomed. Eng. - Appl. Basis Commun.*, Vol. 31, No. 03, p. 1950024, (2019).

[14] M. Nagargoje and R. Gupta, "Effect of sinus size and position on hemodynamics during pulsatile flow in a carotid artery bifurcation," *Comput Methods Programs Biomed.*, Vol. 192, p. 105440, (2020).

[15] T. Martens, Blood flow simulation in carotid arteries with computational fluid dynamics, Bachelor thesis, University of Twente, (2022).

[16] H. JE, "Guyton and Hall textbook of medical physiology," *Philadelphia, PA: Saunders Elsevier*, Vol. 107, p. 1146, (2011).

[17] N. Kumar, R. Pai, S. Abdul Khader, S. Khan and P. Kyriacou, "Influence of blood pressure and rheology on oscillatory shear index and wall shear stress in the carotid artery," *J Braz Soc Mech Sci Eng*, Vol. 44, No. 11, pp. 1-16, (2022).

[18] H. Xie, K. Kim, S. R. Aglyamov, S. Y. Emelianov, M. O'Donnell, W. F. Weitzel, S. K. Wrobleski, D. D. Myers, T. W. Wakefield and J. M. Rubin, "Correspondence of ultrasound elasticity imaging to direct mechanical measurement in aging DVT in rats," *Ultrasound Med. Biol.*, Vol. 31, No. 10, pp. 1351-1359, (2005).

[19] C. Schmitt, A. H. Henni and G. Cloutier, "Characterization of blood clot viscoelasticity by dynamic ultrasound elastography and modeling of the rheological behavior," *J. Biomech.*, Vol. 44, No. 4, pp. 622-629, (2011).

[20] F. Mirakhorli, B. Vahidi, M. Pazouki and P. T. Barmi, "A fluid-structure interaction analysis of blood clot motion in a branch of pulmonary arteries," *Cardiovasc. Eng. Technol.*, Vol. 14, No. 1, pp. 79-91, (2022).

[21] J. Donea, A. Huerta, J. P. Ponthot, and A. Rodríguez-Ferran, "Arbitrary l agrangian–e ulerian methods," *Encyclopedia of Computational Mechanics Second Edition*, pp. 1-23, (2017).

[22] D. Stutts, "Analytical dynamics: Lagrange's equation and its application–a brief introduction," *Missouri S&T.*, Vol. 28, p. 2017, (1995).

[23] K.-J. Bathe and H. Zhang, "A mesh adaptivity procedure for CFD and fluid-structure interactions," *Comput Struct.*, Vol. 87, No. 11-12, pp. 604-617, (2009).

[24] R. Torii, M. Oshima, T. Kobayashi, K. Takagi and T. E. Tezduyar, "Fluid–structure interaction modeling of blood flow and cerebral aneurysm: significance of artery and aneurysm shapes," *Comput. Methods Appl. Mech. Eng.*, Vol. 198, No. 45-46, pp. 3613-3621, (2009).

[25] H. Gharahi, B. A. Zambrano, D. C. Zhu, J. K. DeMarco and S. Baek, "Computational fluid dynamic simulation of human carotid artery bifurcation based on anatomy and volumetric blood flow rate measured with magnetic resonance imaging," *Int J Adv Eng Sci Appl Math.*, Vol. 8, No. 1, pp. 46-60, (2016).

[26] N. Kumar, R. Pai, M. Manjunath, A. Ganesha and S. Abdul Khader, "Effect of linear and Mooney–Rivlin material model on carotid artery hemodynamics," *J. Braz. Soc. Mech. Sci. Eng.*, Vol. 43, No. 8, pp. 1-10, (2021).

[27] D. L. Fry, "Acute vascular endothelial changes associated with increased blood velocity gradients," *Circ. Res.*, Vol. 22, No. 2, pp. 165-197, (1968).

[28] J. J. Paszkowiak and A. Dardik, "Arterial wall shear stress: observations from the bench to the bedside," *Vasc Endovascular Surg.*, Vol. 37, No. 1, pp. 47-57, (2003).

[29] Y.-c. Fung, *Biomechanics: mechanical properties of living tissues*. Springer Science & Business Media, (2013).

[30] V. Tutwiler, J. Singh, R. I. Litvinov, J. L. Bassani, P. K. Purohit and J. W. Weisel, "Rupture of blood clots: Mechanics and pathophysiology," *Sci. Adv.*, Vol. 6, No. 35, p. eabc0496, (2020).

[31] Y. Liu, Y. Zheng, A. S. Reddy, D. Gebrezgiabhier, E. Davis, J. Cockrum, J. J. Gemmete, N. Chaudhary, J. M. Griauzde and A. S. Pandey, "Analysis of human emboli and thrombectomy forces in large-vessel occlusion stroke," *J. Neurosurg.*, Vol. 134, No. 3, pp. 893-901, (2020).

[32] L. Richards, "Presence of large-vessel occlusion predicts outcome for stroke patients," *Nat. Rev. Neurol.*, Vol. 5, No. 12, pp. 636-636, (2009).

[33] A. Hammoud, E. Y. Sharay and A. N. Tikhomirov, "Newtonian and non-Newtonian pulsatile flows through carotid artery bifurcation based on CT image geometry," *AIP Conf. Proc.*, Vol. 2171, No. 1, p. 110022, (2019).

How to cite this paper:

Pouria Talebibarmi and Bahman Vahidi, "3D numerical analysis of arterial thromboembolism through carotid bifurcation,", *J. Comput. Appl. Res. Mech. Eng.*, Vol. 13, No. 1, pp. 13-25, (2023).

DOI: 10.22061/JCARME.2023.8916.2202

URL: https://jcarme.sru.ac.ir/?_action=showPDF&article=1881